RSC Advances

PAPER

View Article Online
View Journal | View Issue

Cite this: *RSC Adv.*, 2014, **4**, 12342

Polyaniline nanotubes with rectangular-hollow-core and its self-assembled surface decoration: high conductivity and dielectric properties†

Pradip Paik,* Ramesh Manda, Chander Amgoth and K. Santhosh Kumar

Received 29th November 2013
Accepted 13th January 2014

DOI: 10.1039/c3ra47155a

www.rsc.org/advances

Polyaniline (PANI) nanotubes with a rectangular hollow core and decorated outer surface-wall with self-assembled nanobeads and triangular flakes of PANI have been synthesized in the presence of ZnO NPs by a sonochemical approach. This is the first example of the formation of well-defined hollow PANI nanotubes with a rectangular hollow interior. The hollow PANI nanotubes have an average length of *ca.* 10 μm and a hollow core with rectangular geometry. Nanobeads of PANI with diameter *ca.* 50 nm have been decorated/self-assembled on the surface of the outer wall of rectangular hollow PANI nanotubes to obtain a "*Date-tree-like*" 3D structure. The crystal structure has been characterized through XRD. The conduction bands and electronic environment have been confirmed through Raman, FT-IR, UV-Vis-NIR, XPS and EPR. Impedance measurements of rectangular hollow PANI nanotubes demonstrate their higher electrical conductivity ($\sigma = 1.1 \pm 0.1 \times 10^{-4}$ S m^{-1} to $3.0 \pm 0.23 \times 10^{-3}$ S m^{-1}) and dielectric properties, depending on the frequency range compared to the PANI particles synthesized in the presence of H^+ and solid PANI fibres. PANI nanotubes with this novel rectangular hollow core structure and surface decorated texture are a unique type of nanostructure, which can be used in various conductive polymer based device applications.

1 Introduction

Since their discovery in 2001 by Nobel Prize winners Shirakawa, MacDiarmid, and Hegger,[1] the conducting polymer has become a powerful platform for potential applications in erasable information storage, shielding of electromagnetic interference, radar-absorbing materials, sensors, indicators, actuators, rechargeable batteries, non-linear optical devices, antistatic coatings and light emitting diodes,[1–3] including drug delivery[4,5] and energy storage devices.[6,7] Conducting polymer nanofibers have attracted researchers because of their improved performance[1–7] with respect to their bulk counterparts.[8,9] In our recent published work we reported on the enhancement of physical properties of the nematic liquid crystal (LC) by doping of conductive PANI nanofibers, which can be used as a magnetically-steered-LC-PANI-nanofiber switch.[9] To date, many attempts have been made to modify nanoparticles/nanofibers of polymeric (organic)/inorganic materials by introducing porosity through template synthesis,[10] conjugating organic moieties by molecular imprinting (MI),[11] and coatings with metal nanoparticles[12] *etc.* in structures, which could impart additional functionality to the solid nanostructures, such as selective sensing, optical activity *etc.* Sensing properties based on the conductivity of polymer nanofibers show promising potential applications in industrial and biomedical applications, including clinical assaying, detection of explosive, chemicals and hazard monitoring.[13] However, their selective detection efficiency is not satisfactory and moreover it depends on the working conditions such as temperature, partial pressure and concentration of the molecules under detection and on the structural alignment of the nanofibres and on the conductivity. 1D conducting polymer nanofibers can be synthesized by many routes, such as insoluble hard templating (*e.g.*, zeolites),[14] soluble soft templating (*e.g.*, surfactants/micelles),[15,16] seeding[17] and biomolecules,[18] which can orchestrate the growth of the 1D nanostructure of the nanofibers, but all of them have a solid core or a circular hollow core. Moreover, the use of conducting polymer is strongly associated with the limiting factors, such as oxidation states, surface textures and morphology, internal structure (like solid or hollow *etc.*), alignment of the backbone chains, extent of doping with ionic solids, space charge polarization and the extent of free electron hopping. PANI is usually synthesized by chemical oxidation polymerization of aniline in

School of Engineering Sciences and Technology, University of Hyderabad, Hyderabad 500 046, India. E-mail: ppse@uohyd.ernet.in; paik@uohyd.ac.in; pradip.paik@gmail.com; Tel: +91-40-2313-4457

† Electronic supplementary information (ESI) available: Fig. S1: PANI flakes formed when the [aniline] : [HCl], and [ASP] : [aniline] were kept at 1 : 1 and 1 : 2, respectively (Batch-1); Fig. S2: PANI0 synthesized in H^+ only; Fig. S3: TGA of PANI0, PANI@AuNPs/Au^{3+} and PANI@ZnO NPs/Zn^{2+}; Fig. S4: Raman spectra for PANI0, PANI@AuNPs/Au^{3+} and PANI@ZnO-NPs/Zn^{2+}; Fig. S5: XPS spectra for PANI@AuNPs/Au^{3+}; Fig. S6: XPS spectra for PANI0 and Fig. S7: XPS spectra for PANI@AuNPs/Au^{3+}. Tables S1–S3, the XPS results for PANI@AuNPs/Au^{3+}, PANI0 and PANI@AuNPs/Au^{3+}, respectively. See DOI: 10.1039/c3ra47155a

aqueous solution in the presence of strong acid (pH < 2) and the strong oxidant ammonium persulfate (APS).[19] PANI nanotubes with a circular hollow core can also be synthesized by chemical oxidation in the presence of various inorganic acids and sulfonic acids,[20] organic acids,[21] polymeric acids,[22] sulphonated CNTs[23] and dendrons.[24] Synthesis of PANI nanotubes with a circular hollow core in the presence of TiO_2 has also been reported.[25] PANI exists in various acid–base and redox forms and their chemical and physical properties depend substantially on their oxidation states. Only the emerald in the salt form (Scheme 1a) of PANI is conducting in nature ($\sigma \sim 10^{-3}$ S m^{-1}).[26]

In this work, we report the innovation of a nanoparticle-based synthesis method of PANI 1D nanotubes with a rectangular hollow interior and surface decorated 3D architecture of nanotubes having very high electrical conductivity and dielectric properties. According to this new procedure, we took ZnO nanoparticles as a template in a homogeneous mixture of highly pure aniline in water and performed acid catalyzed sonochemical polymerization. We are able to create a well-defined 1D PANI with a rectangular hollow interior along the centre of each fiber under controlled conditions. By controlling the sonochemical reaction conditions, the surface of the PANI tubes has been decorated with spherical PANI nanobeads and subsequently architectured stepwise with triangular shaped PANI flakes *in situ*. Finally a "*Date-tree-like*" 3D structure has been designed, which is highly conducting compared to the solid PANI fibers and PANI nanoparticles. Similarly, we have performed the sonochemical reaction in H^+ in the presence of Au nanoparticles with equimolecular weight in two different batches and it never formed a triangular hollow PANI nanostructure. The results have been compared with the solid nanofibers of PANI and PANI nanoparticles.

In an earlier work, Ihee and co-workers have reported on the formation of microtubes of β-peptide tetramer (*trans*-(*S*,*S*)-aminocyclopentane carboxylic acid tetramer), which has a rectangular cross-section (sub-micrometer), by the evaporation induced self-assembly method.[27] To the best of our knowledge the present work is the first report on polyaniline nanotubes with a rectangular hollow interior and decorated outer surface wall with self-assembled PANI nanobeads and triangular flakes, synthesized in the presence of ZnO NPs by a sonochemical approach. Furthermore, this work has been focused on the study of the physical properties, such as crystal structure, conductivity and dielectric properties of polyaniline nanotubes

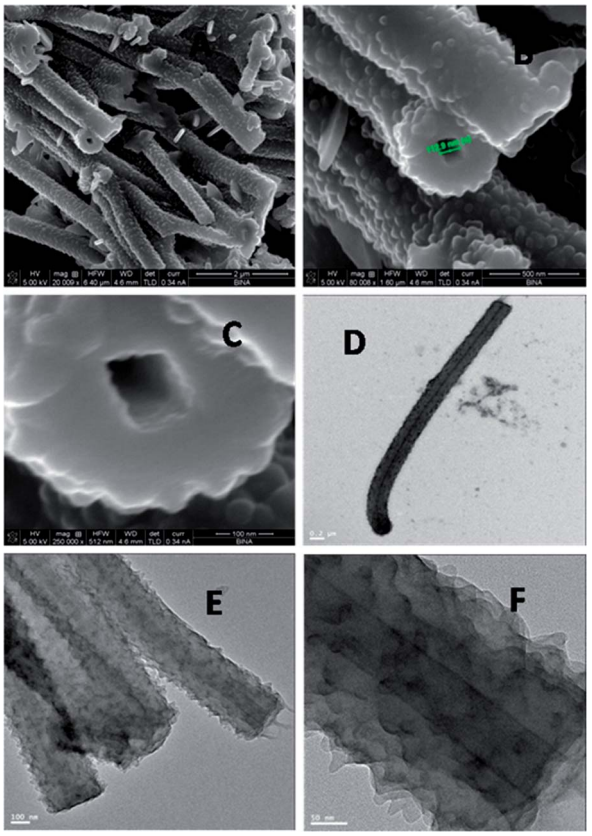

Fig. 1 (A)–(C) FIB images; (D)–(F) HRTEM images of PANI nanotubes with a rectangular hollow interior synthesized in the presence of ZnO NPs.

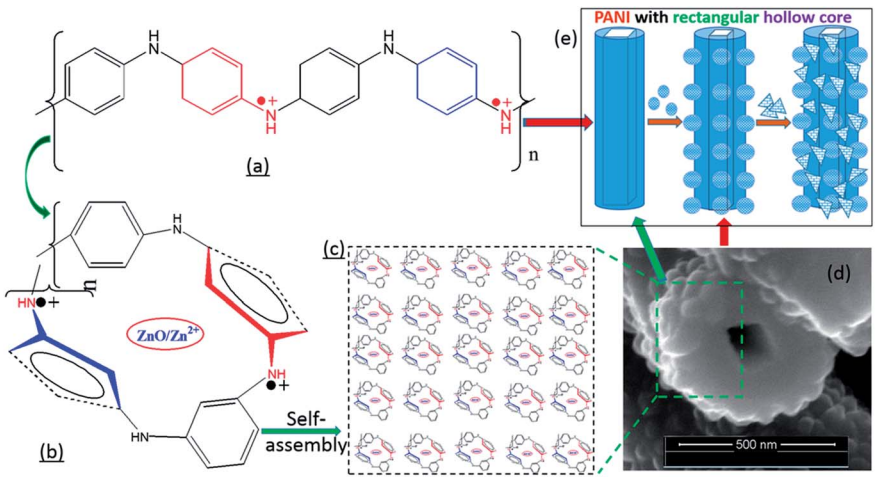

Scheme 1 (a) Structure of conducting emeraldine salt of PANI, (b) possible rearrangement of PANI backbone (c) self-assembly of PANI in presence of ZnO/Zn^{2+}, (d) cross section view of rectangular hollow core and (e) step-wise decoration of PANI with rectangular hollow core.

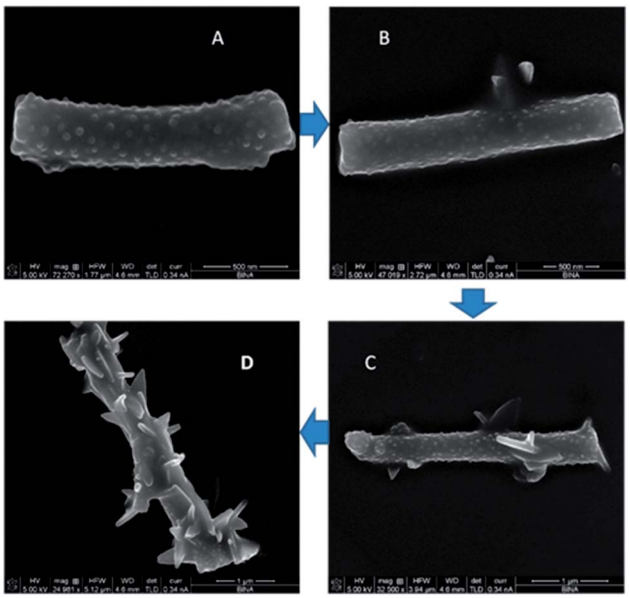

Fig. 2 FIB images of hollow PANI nanotubes (A) surface decorated with spherical nanobeads of PANI (sample-1 for decoration, synthesized with ZnO NPs), (B–D) surface decorated with PANI nanoflexes (sample-2 for decoration synthesized with ZnO NPs, step-2), and (C) surface decorated with PANI nanoflexes (dense flexes) synthesized with ZnO NPs, (from A to D sequential steps).

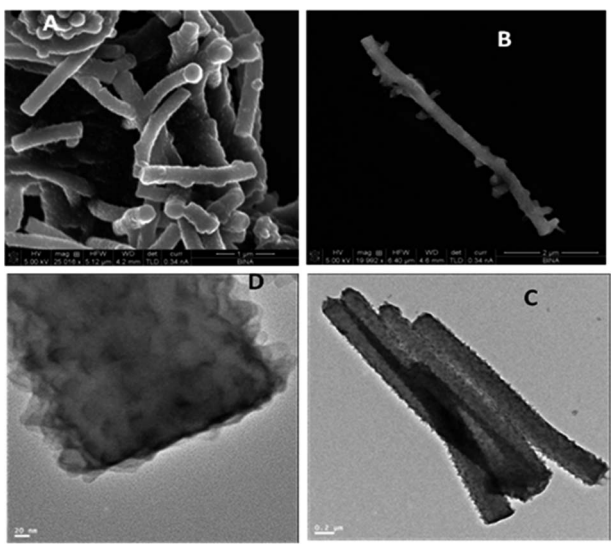

Fig. 3 (A) and (B) FIB micrograph and (C) and (D) HRTEM of PANI nanofibers synthesized in the presence of Au NPs.

with a rectangular hollow interior. The results are very interesting from the application point of view.

2 Experimental

2.1 Materials and reagent

Aniline (>99.5% Sigma-Aldrich), ammonium persulphate (APS, $NH_4S_2O_8$, >98.5%, Sigma), $HAuCl_4$ (99.999%, Aldrich), sodium borohydrate ($NaBH_4$, >99%, Sigma) and ZnO nanoparticles (<50 nm diameter, 97%, Aldrich) were purchased and used as received without further purification.

Table 1 Results obtained from the XRD: *d*-spacing (Å) and (*hkl*) indexing against 2θ (deg.)

PANI@ZnO-NPs/Zn^{2+}			PANI0			PANI@AuNPs/Au^{3+}		
2θ	'*d*' spacing	(*hkl*)	2θ	'*d*' spacing	(*hkl*)	2θ	'*d*' spacing	(*hkl*)
6.44	13.7	—	8.82	10.01	—	6.27	14.01	—
18.01	4.92	(002)	15.33	5.78	(101)	18.20	4.87	(110)/(002)
19.89	4.46	(012)	20.44	4.32	(012)	20.02	4.43	(012)
25.36	3.51	(200)	25.25	4.35	(012)	25.06	3.48	(112)/(200)
28.65	3.11	(211)				29.10	3.10	(211)
33.10	2.70	(212)				41.14	2.19	(114)/(221)
34.79	2.56	(131)/(123)						
41.44	2.19	(114)/(221)						

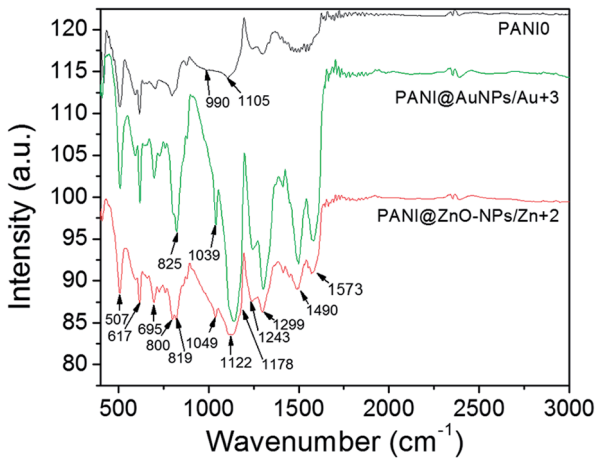

Fig. 4 FTIR spectra for PANI0, PANI@AuNPs/Au^{3+} and PANI@ZnO-NPs/Zn^{2+}, showing the molecular structure and chemical bonding responsible for the conductivity.

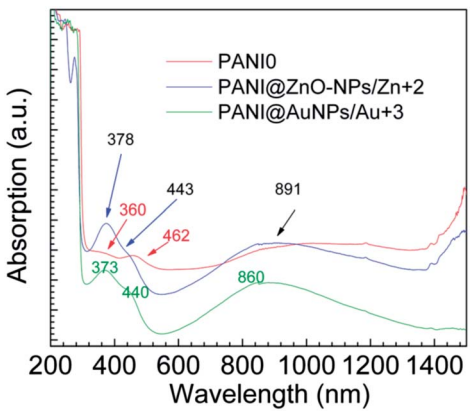

Fig. 5 UV-Vis-NIR spectra for PANI0, PANI@AuNPs/Au^{3+} and PANI@ZnO-NPs/Zn^{2+}, showing conduction and non-conduction bands.

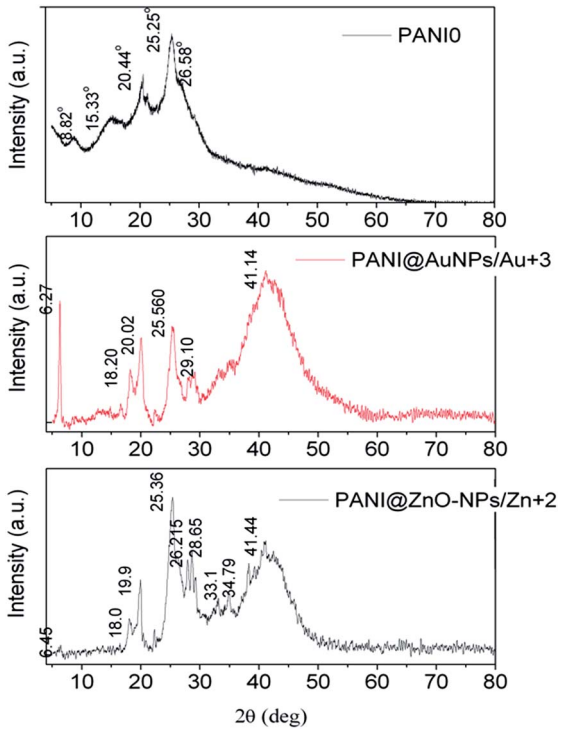

Fig. 6 XRD patterns for PANI0, PANI@AuNPs/Au^{3+} and PANI@ZnO-NPs/Zn^{2+}.

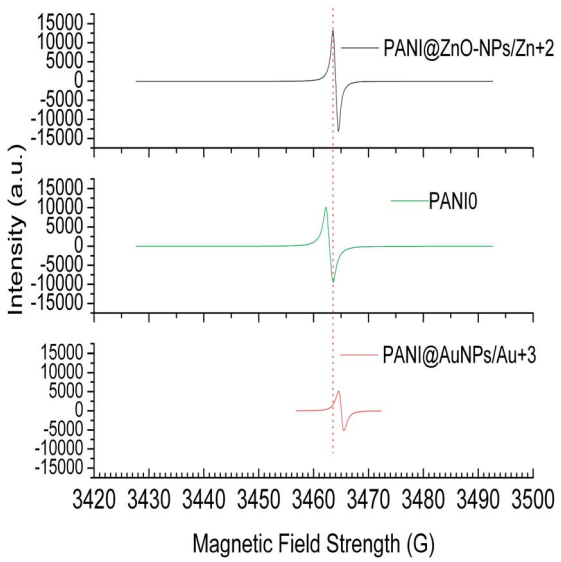

Fig. 7 EPR spectra for PANI0, PANI@AuNPs/Au^{3+} and PANI@ZnO-NPs/Zn^{2+}.

2.2 Synthesis of functionalized polyaniline nanotubes (hollow and surface decorated)

2.2.1 Synthesis of Au nanoparticles. A 90 ml (0.1 mM) solution of $HAuCl_4$ was prepared. Aqueous $NaBH_4$ (10 ml, 0.1 g) was immediately added to the above solution and stirring continued for 1 h. The solution changed to a light brown colour with the addition of $NaBH_4$ solution. The reaction was

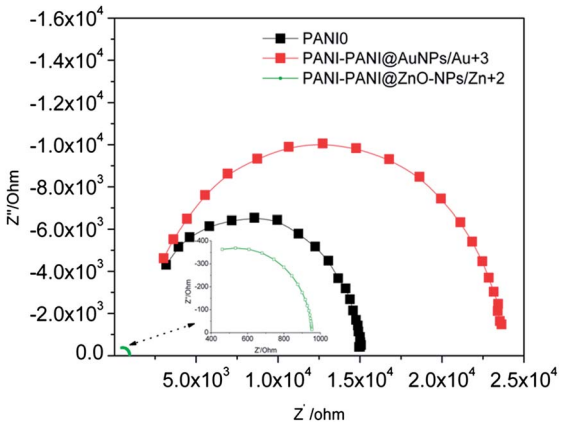

Fig. 8 Cole–Cole plot for PANI0, PANI@AuNPs/Au^{3+} and PANI@ZnO-NPs/Zn^{2+}. Inset is the enlarged view for PANI@ZnO-NPs/Zn^{2+}.

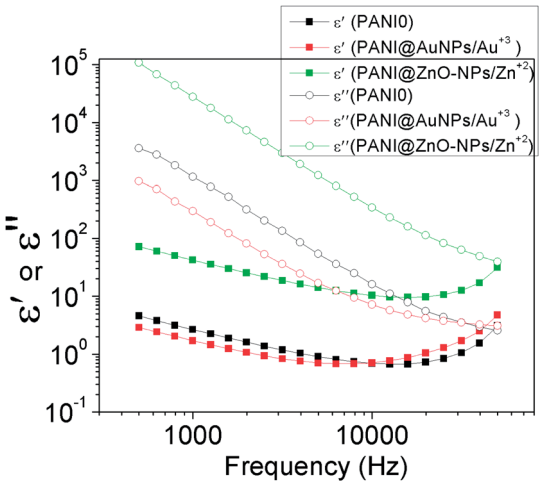

Fig. 9 Frequency dependence of relative dielectric constants ε' and the relative dielectric loss ε'' for PANI0, PANI@AuNPs/Au^{3+} and PANI@ZnO-NPs/Zn^{2+}.

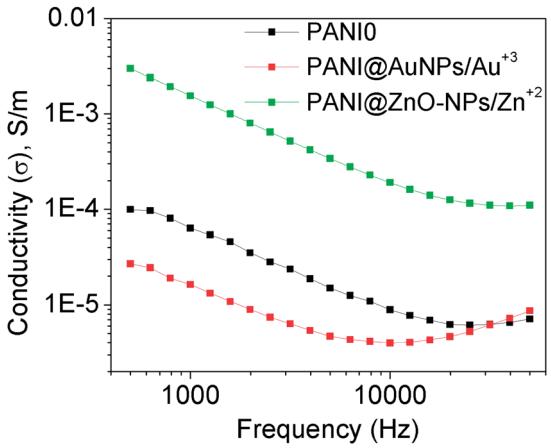

Fig. 10 Frequency dependence of the conductivity of PANI@ZnO-NPs/Zn^{2+}, PANI0 and PANI@AuNPs/Au^{3+}.

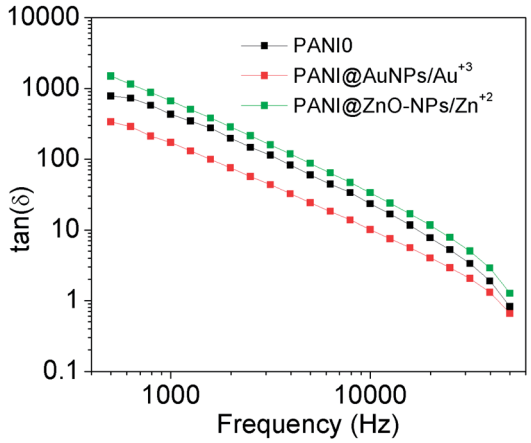

Fig. 11 Frequency dependence of tan δ for PANI@ZnO-NPs/Zn^{2+}, PANI0 and PANI@AuNPs/Au^{3+}.

continued overnight to reach completion, resulting in a red-wine colour. The Au solution was dialyzed against deionized water for 24 h in a 12.5 kDa dialysis membrane, with intermittent changing of water to purify it, and lyophilized to obtain a dry powder, which was readily dispersible in water.

2.2.2 Sonochemical synthesis of functionalized polyaniline nanofibers in the presence of Au. PANI was synthesized by an aqueous solution polymerization method. A typical synthesis method is as follows: 0.373 g (4 mmol) aniline was mixed in 20 ml deionized water in which 0.01 mg Au nanoparticles (dia ~ 10–15 nm) was added. The mixture was sonicated for 30 s in an ice bath to form a homogeneous mixture. A fresh solution of ammonium persulphate (APS, 0.9 g in 2 ml ice water) and a pre-cooled 10 ml HCl (1 M) were added rapidly into the premixed aniline–Au solution. Then the mixture was sonicated for 5 s in an ice bath and subsequently kept at 0 °C for 24 h. The crude product was dialysed for 24 h against deionized water until a neutral solution was obtained. The dialysis assisted in the removal of chloroaurate and other ions. Purified PANI was then lyophilized to obtain dry powder, which is readily redispersible in water. This is a solid (not hollow) powder, black in colour, and is designated as PANI@AuNPs/Au^{3+}.

2.2.3 Sonochemical synthesis of polyaniline nanotubes with rectangular hollow core in the presence of ZnO

Polyaniline nanofibers in the presence of ZnO. A similar procedure was followed to achieve PANI using ZnO (as prepared in the presence of Au NPs). A brief synthesis method is as follows: 0.373 g (4 mmol) aniline was mixed in 20 ml deionized water in which 0.01 mg ZnO nanoparticles (dia ~ 30–40 nm) was added and sonicated for 30 s at 0 °C. An APS solution (0.9 g in 2 ml ice cold water) and a pre-cooled 10 ml HCl (1 M) were added rapidly into the premixed aniline–ZnO solution. Then the mixture was sonicated for 5 s in an ice bath and subsequently kept at 0 °C for 24 h. The crude product was dialysed against deionized water until a neutral solution was obtained. The dialysis assisted in the removal of Zn^{2+}, Cl^- and other ions. Then the purified PANI was lyophilized to obtain a dry powder, which is readily dispersible in water. This powder obtained is hollow nanofibers, black in colour and designated as PANI@ZnO-NPs/Zn^{2+}.

Functionalized and decorated polyaniline nanotubes prepared in the presence of ZnO NPs. In the second stage, 100 mg PANI (prepared with ZnO) was taken up in 50 ml deionized water. Then 1 mmol aniline was added, followed by a desired amount of HCl (1 M) to make a 1 : 1 [aniline] : [HCl] solution. Then the required amount (0.25 g) of APS was added (molar ratio of [ASP] to [aniline] is ~1 : 2). Then the reaction mixture was stirred at 75 °C in a water bath and kept for 10 min to ensure uniform temperature distribution throughout the reaction mixture followed by sonication for 5 s. Then APS was dissolved and the solution turned into deep green to black. Then the reaction vessel was kept in a closed chamber at 0 °C without agitation for 24 h. Then it was dialyzed against deionized water until a neutral solution was obtained. Purified functionalized PANI was then lyophilized to obtain a dry powder. These hollow PANI nanofibers are decorated with flakes and are black in colour and designated as PANI@ZnO-NPs/Zn^{2+}.

Similarly, PANI nanoparticles were prepared in the absence of any other metal salt or nanoparticles other than H^+ and APS and the sample is designated as PANI0.

2.3 Characterizations

The high resolution images were acquired with HRTEM (JEOL JEM-2100 electron microscope) using an accelerated voltage of 200 kV. High resolution focused ion beam (FIB) images were acquired using a FEI Helios 600 system using an accelerated voltage of 5 kV. We used a BRUKER AXS D8 ADVANCE Diffractometer (using Cu-Kα $\lambda = 1.5418$ Å radiation) operating at 40 kv/40 mA, with a graphite reflected beam monochromator and variable divergence slits for powder X-ray diffraction analysis. Data were collected from 10 to 60° (2θ) with a resolution of 0.02°. The FT-IR spectra were recorded with a VARIAN spectrophotometer at room temperature with KBr pellets. Thermogravimetry analysis (TGA) measurements were performed with a Thermo ONIX Gaslab 300 TGA instrument from 30–1000 °C in an N_2 atmosphere. In order to detect the free radicals

Table 2 Frequency dependence of conductivity of PANI@ZnO-NPs/Zn^{2+} at different temperature

Frequency (Hz)	5×10^2	10^3	10^4	2×10^4	5×10^4
σ (30 °C)	2.98×10^{-3}	1.55×10^{-3}	1.88×10^{-4}	1.23×10^{-4}	1.10×10^{-4}
σ (45 °C)	1.07×10^{-3}	8.61×10^{-4}	1.09×10^{-4}	7.45×10^{-5}	7.02×10^{-5}
σ (60 °C)	6.39×10^{-4}	3.36×10^{-4}	4.71×10^{-5}	3.86×10^{-5}	4.37×10^{-5}

present in the sample, the electron spin resonance (EPR) spectroscopy measurements were performed on a Bruker EPR 100d X-band spectrometer ($\upsilon = 9.77$ GHz) ,with a 100 KHz magnetic field modulation (ER083CS). Raman spectra for polyaniline nanofibers were recorded on a JobinYvon Horiba Raman System. The 632.8 nm line of a He–Ne laser is used as the excitation source, focused to a 1–2 μm spot size. The UV-Vis-NIR spectra were recorded on a CARY 100 Scan UV-Vis-NIR spectrometer. The oxidation states of the polyaniline samples were investigated by X-ray photoelectron spectroscopy (XPS) measurements on a KRATOS AXIS HS spectrometer using Al KR radiation. The C 1s (binding energy 284.6 eV) peak was chosen as a reference line for the calibration of the energy scale. The bulk conductivity of the polyaniline samples was determined by impedance measurements in the frequency range 25 kHz to 100 Hz.

3 Results and discussions

Size and morphology: Scheme 1 is showing a possible mechanism for the formation of PANI nanotubes with a rectangular hollow interior. Fig. 1(A)–(C) show the FIB micrographs for PANI nanotubes with rectangular hollow interior at various magnifications. They were synthesized by polymerization of aniline in acidic conditions (H^+), with templating of the ZnO-NPs at 0 °C, and are designated as PANI@ZnO-NPs/Zn^{2+}, since ZnO NPs become colourless in HCl solution and the following ionic dissociation occurs: ZnO → Zn^{2+}. The details of the synthesis method for PANI@ZnO-NPs/Zn^{2+} nanotubes are explained in the experimental section. In order to understand the detailed architecture of the PANI@ZnO-NPs/Zn^{2+} nanotubes, HRTEM experiments were employed at various magnifications (Fig. 1(D)–(F)). Both FIB and HRTEM investigations revealed that the PANI@ZnO-NPs/Zn^{2+} nanotubes are hollow in nature. Microscopy analysis as well ensured that the PANI@ZnO-NPs/Zn^{2+} nanofibers have a rectangular hollow core structure with an average geometrical dimension of the core being ~112 nm × ~100 nm with a wall thickness of ~120 nm. The average length of the PANI@ZnO-NPs/Zn^{2+} nanotubes has been found to be ~10 μm, with an average outer diameter of ~350 nm. FIB inspection revealed that the surfaces of the rectangular hollow PANI@ZnO-NPs/Zn^{2+} are decorated with the spherical PANI nanobeads. The beads are spherical in shape and their diameter is about 50 nm. These PANI@ZnO-NPs/Zn^{2+} nanotubes were taken for further stepwise decoration on the surface with extended flakes in stereo space.

Fig. 2(A)–(C) are showing a clear change in morphology and surface decoration and their gradual change in the number density of the functionalized nanobeads and flakes. To understand the stepwise decoration of PANI@ZnO-NPs/Zn^{2+} nanofibers by polyaniline flakes, we performed three individual batches of reactions. Batch-1: only 1 mmol aniline was taken with the required amounts of ASP and HCl, and the molar ratios of [aniline] : [HCl] and [ASP] : [aniline] were kept at 1 : 1 and 1 : 2, respectively. Batch-2: 50 mg PANI@ZnO-NPs/Zn^{2+} nanotubes was taken with 1.5 mmol aniline and the required amounts of HCl and ASP were added to it; [aniline] : [HCl] and [ASP] : [aniline] were kept at 1 : 1 and 1 : 2, respectively. Batch-3: 50 mg dried and purified sample from Batch-2 was taken with 1.5 mmol aniline with the required amounts of HCl and ASP to make the molar ratio of [aniline] : [HCl] to be 1 : 1, and the molar ratio of [ASP] : [aniline] to 1 : 2. All the reactions were carried out under the same conditions at 0 °C without agitation for 24 h. For the Batch-1 reaction, only flakes are formed (Fig. S1†). For the Batch-2 reaction, the flakes are decorating the surface of the PANI@ZnO-NPs/Zn^{2+} nanotubes (Fig. 2B). The population density of the flakes on the surface of the rectangular hollow PANI@ZnO-NPs/Zn^{2+} is found to be less. For the Batch-3 reaction, flakes are decorated on the surface of the PANI@ZnO-NPs/Zn^{2+} nanotubes (Fig. 2C) and the number of flakes on the surface of the PANI@ZnO-NPs/Zn^{2+} tubes is relatively high compared to the sample obtained from the Batch-2 reaction. This clearly indicates that, on increasing the aniline amount in the decoration process, the surface morphology of the rectangular hollow PANI@ZnO-NPs/Zn^{2+} nanofibers is regulated by the additional number of flakes. In fact, the flakes have grown on the surface of the hollow PANI@ZnO-NPs/Zn^{2+} nanotubes.

Earlier, a number of formation mechanisms of nanofibers of conducting polymers was reported by a group of researchers.[15–18,28,29] Polyaniline nanostructures such as nanowires/-fibers/-rods/-tubes can be synthesized by introducing 'structural directors', such as soft templates (*e.g.* surfactants, micelles),[15,16] organic dopants,[17] biomolecules[18] *etc.*, which can organize the growth of the nanofibers, but none of their hollow structures are rectangular in shape. Recently, it has also been found that the introduction of small amount of dimers/oligomers into the polymerization reactions can control the growth of the fibers.[28] The amount of mer units, oxidizer (APS) and catalyst (H^+) present in the reaction process can regulate whether it will form fibers or flakes.[29] However, to the best of our knowledge the formation of surface engineered nanotubes with a rectangular hollow interior and decorated by flakes in systematic steps is an advancement in the design of conductive polymers and has not been reported earlier. Therefore, nanostructures have been decorated by introducing ZnO/Zn^{2+} in the reaction mixture. Without the introduction of Au/Au^{3+} or ZnO/Zn^{2+} in the reaction mixture it forms the spherical shaped submicron sized PANI particles with nanopillars on the surface of the spheres, even though all the other reaction conditions remain the same (PANI0, see Fig. S2†).

Fig. 3(A) and (B) show the FIB micrographs for a branch of PANI nanofibers and a single nanofiber, respectively, which have been synthesized by the polymerization of aniline in acidic conditions (H^+), by templating the Au NPs at 0 °C. A colloidal solution of Au NPs was added in 1 (M) HCl solution, the red-pink colour of the solution becomes colourless due to the electronic transition: Au^0 → Au^{3+}, and hence we have designated the final product as PANI@AuNPs/Au^{3+}.

In order to understand the construction of the PANI@AuNPs/Au^{3+} nanofibers, HRTEM was employed at both lower and higher magnifications, Fig. 3(C) & (D), respectively. Both FIB and HRTEM show that the PANI@AuNPs/Au^{3+} nanofibers are solid, *i.e.* the obtained polyaniline fibers do not have any

hollow interior. Microscopy analysis also revealed that the PANI@AuNPs/Au^{3+} nanofibers have an average length of about 10 μm with an average diameter of ~250 nm. The idea of adding Au nanoparticles in the synthesis is to achieve the highly oriented solid PANI in a metallic ionic medium (Au^{3+}).

Formation mechanism of rectangular hollow PANI@ZnO-NPs/Zn^{2+} nanotubes: The difference in this formation of functionalized PANI nanofibers/tubes, compared to other methods, is that it is a two-step process. The first step is the atomization of aniline at 0 °C to form PANI molecules, followed by crystal growth at the same temperature in the ZnO/Zn^{2+} system (Fig. 2). Secondly, we allowed the PANI flakes to grow on the surface of the rectangular-hollow-core PANI nanotubes at 0 °C. If the polymerization of aniline is allowed to form PANI in the temperature range 75–80 °C, followed by crystal growth, then the PANI chains are not able to grow effectively to form 1D nanofibers, due to the high solubility of aniline at such a high temperature.[29]

If polymerization occurs followed by crystal growth between 0 and 5 °C, even then PANI crystals could not grow effectively in a 1D direction. If polymerization is allowed at higher temperatures, for example at 75–80 °C followed by crystal growth in between 0 and 5 °C, then it leads to the formation of oriented solid PANI fibers.[29] The introduction of a small number of dimers/oligomers into the polymerization reactions can control the growth of the conducting polymer nanofibers.[28] When polymerization of aniline in the presence of the ZnO/Zn^{2+} ionic system under ultrasonication is allowed and is combined with crystal growth at 0 °C, then the highly fascinated and oriented PANI 1D nanotubes with rectangular hollow interiors are formed in high yield. Whenever we have allowed polymerization of aniline in the presence of Au/Au^{3+} under ultrasonication, followed by crystal growth at 0 °C, the highly oriented PANI 1-D nanofibers are formed but without any hollow core. There is an obvious question: what is the role of Au/Au^{3+} or ZnO/Zn^{2+}?

We observed that the presence of Au/Au^{3+} controls the high orientation of the PANI fibers and helps the fibers to grow in 1D without forming any hollow structure in the centre of the fibers, even though all other synthetic conditions remain the same. The absence of any NPs or ions (Au/Au^{3+} ions or ZnO/Zn^{2+}) leads to the formation of uncontrolled growth of the fibers with irregular surface morphology. Additionally, polymerization of aniline in the presence of ZnO/Zn^{2+} leads to the formation of PANI nanotubes with a rectangular hollow core and the formation of well-defined rectangular hollow interiors of nanotubes of conductive polymer (*i.e.* PANI), following the self-assembling intermolecular arrangement mechanism of polymer chains along the longitudinal direction. Although in some cases the formation of micron sized fibers with β-peptide and other aromatic molecules has been reported, those with a hollow-rectangular cross-sectional interior have not been reported.[27,30]

It is worth mentioning that the concentration of aniline and H^+ are important parameters to control the growth of polyaniline at 0 °C. When the temperature is 0 °C and the reaction is in progress, the concentration of H^+ in the reaction medium reaches zero at a certain stage and the concentration of polyanilinium salt also decreases or does not form further, due to the lack of H^+ ions. This situation leads to the formation of spherical crystal beads of PANI, which we are able to create on the surface of PANI. These PANI nanobeads induce self-assembly on the surface of the rectangular hollow tubes, as observed in Fig. 3(A), such that the distance between the beads is almost the same. In the present work we are able to create the uniform sized and spherical beads of around 50 nm in diameter on the surface of the rectangular hollow PANI nanotubes. The nanobeads are decorated isotropically due to a stabilized ionic environment of oxidised aniline droplets, which have been placed at equal distance on the surface of the fibers. Thus the nanobeads of PANI are self-assembled on the rectangular hollow PANI tubes.

In the stepwise process for the formation and decoration of flakes on the surface of hollow-rectangular PANI tubes (Fig. 3B and C), it is also observed that the formation of flakes and their morphology also depends on the aniline concentration. Typically, for the formation of PANI flakes and their self-assembly on rectangular hollow tubes, the concentration of [aniline] : [H^+] is maintained 1 : 1 with an aniline concentration of as low as 0.8 mmol. In this work it is observed that the thickness of PANI flakes is ~100 nm with triangular shapes. All the triangular flakes are self-assembled on the surface of the rectangular hollow PANI tubes to form a "*Date-tree-like*" 3D structure.

In order to confirm the molecular structure of PANI0, PANI@AuNPs/Au^{3+} and PANI@ZnO-NPs/Zn^{2+}, FT-IR spectroscopy has been performed at room temperature. The FT-IR spectrum of PANI reveals that the bands at 1573 and 1490 cm^{-1} can be attributed due to the deformation (stretching) mode of –C=C– of the quinoid and benzoid rings. The band at 1299 cm^{-1} is assigned to the C–N stretching of the secondary aromatic rings. The band at 1243 cm^{-1} appeared due to the stretching and vibration of the –C–N–C– bonds present in polaron. The band at 1122 cm^{-1} arises due to the bending and vibration of –C–H bonds in the plane. This bond forms during the protonation of aniline during polymerization and broadens towards the higher wave numbers beyond 1178 cm^{-1}. The bands at 695 and 1049 cm^{-1} are the result of outer plane bending of 1,2-rings and 1,2,4-rings, respectively. The peaks in between 800 and 900 cm^{-1} appear due to the *para* substitution of the aromatic rings followed by polymerization, proceeding through the head-to-tail mechanism. The quinoid units are converted to benzoid units upon acid protonation of the emeraldine base by a proton induced spin-unpairing mechanism, therefore no prominent absorption peak appears at around 1380 cm^{-1}. The protonated emeraldine shows a long absorption tail above 1950 cm^{-1}, and an absorption peak appears around 3250 cm^{-1}, due to the stretching of the N–H bonds. The appearance of an intense broad band at 1178 cm^{-1} is associated with the high electrical conductivity and is due to the high degree of delocalization of the free electron in PANI. The results indicate that the broadening of this peak is more for the PANI0 and PANI@ZnO-NPs/Zn^{2+} compared to the PANI@AuNPs/Au^{3+}. The peak broadening for rectangular-hollow PANI@ZnO-NPs/Zn^{2+} is highest among the three different samples. This is also an indication of lower

conductivity of PANI@AuNPs/Au^{3+}, as compared to PANI0 and PANI@ZnO-NPs/Zn^{2+}. The conductivity is high for the rectangular-hollow PANI@ZnO-NPs/Zn^{2+}, which we have found from the impedance study (discussed in separate section). Additional peaks other than the peaks/bands related to the conductivity match with other FT-IR peaks, and are commonly observed for the PANI backbone structure, which is usually obtained by traditional chemical synthesis roots, mainly by acid catalyzed polymerization of aniline.[31,32]

UV-Vis-NIR absorption spectra of PANI0, PANI@AuNPs/Au^{3+} and PANI@ZnO-NPs/Zn^{2+} were conducted in deionised propanol (Fig. 5). The characteristic peaks for PANI0 appear at 360, 462 and 890 nm (long tail), for PANI@AuNPs/Au^{3+} at 378, 443, and 891 nm (long tail), whereas for PANI@ZnO-NPs/Zn^{2+} the peaks appear at 247, 276, 373, 440 and 885 nm (long tail). The absorption spectra in Fig. 5 show that the peaks at 247 nm and 276 nm arise due to the $\pi \rightarrow \pi^*$ transition and the polaron band $\rightarrow \pi^*$ transition of PANI rectangular hollow nanofibers (distinct for PANI@ZnO-NPs/Zn^{2+}), respectively. The peak at 360–378 nm is due to the $\pi \rightarrow \pi^*$ transition in the benzoid ring of the emeraldine base form of polyaniline.[16] The band in between 440 and 462 nm and the extended broad band starting from 580 to 1400 nm are attributed to the $\pi \rightarrow$ localized polaron band.[29] This represents the presence of a major conducting form of emeraldine salts of PANI synthesized with a H^+ catalyst, which have an extended conjugation. The peak at 860 nm corresponds to the emeraldine salt of PANI@AuNPs/Au^{3+} and it might be the possible reason for the shorter conjugation length and hence less conductivity compared to the PANI@ZnO-NPs/Zn^{2+} and PANI0 (absorption band peak at 891 nm and free carrier tail of conjugated electron extended far beyond 1400 nm).[16,29] This could be the possible reason for the high conductivity of rectangular-hollow PANI@ZnO-NPs/Zn^{2+} and PANI0 compared to PANI@AuNPs/Au^{3+}. We have found similar results from the impedance study (discussed in the subsequent section). Due to the electron spin–orbital coupling/overlap of the phenyl ring's π electrons and nitrogen lone pairs, the extent of conjugation decreases and results in lower conductivity for the PANI@AuNPs/Au^{3+} solid fibers compared to the other two samples (PANI@ZnO-NPs/Zn^{2+} and PANI0).

The XRD patterns of PANI0, PANI@AuNPs/Au^{3+} and PANI@ZnO-NPs/Zn^{2+} have been shown in Fig. 6 to distinguish the solid state crystalline structure of the samples. The XRD pattern of PANI0 shows four distinct peaks at $2\theta = 8.82^\circ$ (d spacing = 10.01), 15.33° ($d = 5.78$), 20.44° ($d = 4.32$) and 25.25° ($d = 4.35$). The peak at 20.44° is due to the periodicity of the polymer chains where the PANI chains are parallel to each other. The peaks at $2\theta = 25.25^\circ$ may be attributed to the periodicity of the polymer chains, where the chains are arranged in a perpendicular manner.[33] The XRD pattern for PANI@AuNPs/Au^{3+} shows six distinct peaks at $2\theta = 6.27^\circ$, 18.20°, 20.02°, 25.56°, 29.10° and 41.14°, with a 'd' spacing of about 14.01, 4.87, 4.43, 3.48, 3.10 and 2.19 Å, respectively. For PANI@ZnO-NPs/Zn^{2+}, eight distinct diffraction peaks appear at $2\theta = 6.44^\circ$, 18.01°, 19.89°, 25.36°, 28.65°, 33.10°, 34.79° and 41.44°, with 'd' spacings of 13.7, 4.92, 4.46, 3.51, 3.11, 2.70, 2.56, and 2.19 Å, respectively. The peaks at $2\theta \sim 20.44^\circ$ and $2\theta \sim 25.25^\circ$ are those generally observed for PANI, whereas the peak at $2\theta \sim 6^\circ$ for PANI@AuNPs/Au^{3+} and PANI@ZnO-NPs/Zn^{2+} is observed for the highly ordered crystalline structure of PANI.[34] Usually, PANI synthesized by a conventional acid catalysed (H^+) method does not show any distinct XRD peaks and is amorphous in nature. However, an additional peak for both PANI@AuNPs/Au^{3+} and PANI@ZnO-NPs/Zn^{2+} is observed at $2\theta \sim 41^\circ$, due to the very high orientation of the PANI chains in long range order. In conclusion, the 1D backbone structure of PANI with a very high length/diameter ratio, with surface decoration by nanobeads and nanoflakes (Fig. 1 and 2), is highly crystalline. In the conventional PANI synthesis method, the aniline monomer reacts with HCl to form the anilinium cation and it becomes difficult to crystallize them in a periodic order with vigorous stirring, to produce an amorphous aggregate of anilinium cations. Detailed XRD indexing and results have been calculated[35] and represented in Table 1.

The thermal stabilities of PANI0, PANI@AuNPs/Au^{3+} and PANI@ZnO-NPs/Zn^{2+} were checked with TGA (Fig. S3†). The thermogram clearly shows that the degradation of all samples occurs in three steps. The weight loss at 100 °C is due to the moisture, whereas all the major weight loss is observed at 300 °C. After 500 °C the rate of weight loss of the PANI@AuNPs/Au^{3+} sample is somewhat faster with respect to PANI0, and PANI@ZnO-NPs/Zn^{2+}. This is due to the wide distribution of size of the polymer chains. The low molecular weight PANI polymer chain degrades faster on heating. Faster weight loss is associated with lower M_w (molecular weight) and we can assume that the electronic conjugation length is also smaller for PANI@AuNPs/Au^{3+} compared to the other two samples, PANI0 and PANI@ZnO-NPs/Zn^{2+}.

The conductivity of PANI is strongly associated with its oxidation states. Raman spectroscopy is a very sensitive tool for defining the various oxidation states, and here we have found the conducting states of novel PANI0, PANI@AuNPs/Au^{3+} and PANI@ZnO-NPs/Zn^{2+} samples (Fig. S4†). Our PANI samples are found to be a mixture of both its non-conducting emeraldine base and conducting emeraldine salt forms, as revealed by the FT-IR and UV-Vis-NIR (Fig. 4 and 5). For the PANI0, PANI@AuNPs/Au^{3+} and PANI@ZnO-NPs/Zn^{2+} samples, the band appears at 1350 cm^{-1} because of the presence of the conducting emeraldine salt form and thus the PANI fibers form through the intermediate polysemiquinone radical formation mechanism.[36] The peak at 1580 cm^{-1} appears due to the stretching of –C=C– quinoid, consistent with cross linking for all the synthesized samples.[37] But it is very difficult to calculate the extent of the conducting emeraldine salt present in the samples. However, we have confirmed this from the impedance spectroscopy study.

In order to investigate the free electron responsible for the conductivity of all the PANI samples, EPR experiments were as well as the UV-Vis-NIR experiments (Fig. 5). The EPR spectra corroborate the presence of radical cations, which indicates that the PANI0, PANI@AuNPs/Au^{3+} and PANI@ZnO-NPs/Zn^{2+} samples are conducting (Fig. 7). EPR for PANI0, PANI@AuNPs/Au^{3+} and PANI@ZnO-NPs/Zn^{2+} represent signals at $g = 2.003$. All the samples show a similar shape for the spectra, while PANI@AuNPs/Au^{3+} show peak broadening and a decrease in the

intensity of the peak from PANI@ZnO-NPs/Zn^{2+} to PANI0, and then to PANI@AuNPs/Au^{3+}. The broadening of the peaks in PANI0 and PANI@AuNPs/Au^{3+} are due to the reduction of the diffusion of the unpaired electrons compared to PANI@ZnO-NPs/Zn^{2+}. It is evident that the presence of Na^+, K^+, Ca^{2+} or Mg^{2+} in a composite system of PANI-zeolite/clays hinders the free electron's movement.[38] Thus the occurrence of Zn^{2+} or Au^{3+} during the synthesis of PANI (and their successive removal by solvent treatments) affects the formation of the nanostructure. The complete removal of Zn^{2+} or Au^{3+} is assured by the XPS spectrum study and the results are shown in the ESI, Fig. S5 to S7 and Table S1 to Table S3.† In conclusion, metal ions not only hinder the electron diffusion of the PANI (conducting polymers) but they also influence the extent of formation of the emeraldine salts.

The frequency dependent ($f = 0$ to 50 kHz) dielectric properties and electronic conductivity of PANI@ZnO-NPs/Zn^{2+} have been studied and compared with the results of PANI0 and PANI@AuNPs/Au^{3+} with an open circuit potential of 0V at room temperature (300 K).

Fig. 8 shows the Cole–Cole plots for the dielectric relaxation and revealed that the relaxation obeys the Cole–Cole circular arc law for all three samples, PANI0, PANI@AuNPs/Au^{3+} and PANI@ZnO-NPs/Zn^{2+}. The parallel connected R–C circuit was used as an equivalent scheme of the cell. The relative complex dielectric constant, ε', is calculated by eqn (1)–(3),

$$\varepsilon^* = \varepsilon' - i\varepsilon'' = \left[\frac{C_p^*}{C_o}\right] \quad (1)$$

with empty cell capacity C_o, where

$$\frac{C'_p}{C_o} = \frac{1}{Z'(i\omega)} \times \frac{1}{C_o} = \varepsilon' \quad (2a)$$

$$\frac{C''_p}{C_o} = -\frac{1}{Z''(i\omega)} \times \frac{1}{C_o} = \varepsilon'' \quad (2b)$$

Our sample cell consists of round parallel palates with diameter D (~10 mm) and spacing $d \sim 0.5$ mm. C_o is calculated by the formula:

$$C_o = \varepsilon_o \frac{\pi\left(\frac{D}{2}\right)^2}{d} \quad (3)$$

The frequency dependent ε' (dielectric constant, real part) and ε'' (dielectric constant, imaginary part) have been measured and are represented as a log–log plot in Fig. 9. ε' is determined to be 30 ± 1.5 ($f = 50$ kHz) to 71 ± 2.6 ($f = 500$ Hz) for PANI@ZnO-NPs/Zn^{2+}, which is of very high value compared to PANI0 (minimum 0.6 ± 0.1, maximum 4.4 ± 0.25) and PANI@AuNPs/Au^{3+} (minimum 0.5 ± 0.1, maximum 4.7 ± 0.22). Similarly, it is found (Fig. 9) that the frequency dependent ε'' is very high for PANI@ZnO-NPs/Zn^{2+}, compared to PANI0 and PANI@AuNPs/Au^{3+}. There are different mechanisms for the dielectric response and the electrical conduction in polymers/organic materials. The dielectric relaxation in the ultra low frequency range (10^{-1}–10^{-6} Hz) is usually the result of ionic space-charge polarization[39] or the formation of the electrical double layer at the electrode.[40] The ionic space-charge polarization arises due to the long range movements of the impurity ions in the system. In our system the PANI samples are synthesized in the presence of a H^+ catalyst, which leads to the formation of emeraldine salts, whereas Zn^{2+} has an additional influence. None of our samples showed any data points in Cole–Cole plots between 0 and 400 Hz.

Further, based on the imaginary (ac conductance) ε'' components of the permittivity (ε') data, the frequency-dependent ac current conductivities (σ) of PANI@ZnO-NPs/Zn^{2+}, PANI@AuNPs/Au^{3+} and PANI0 have been determined from 400 Hz to 50 kHz (shown in Fig. 10) using the formula:

$$\sigma = 2\pi\varepsilon_o\varepsilon''f \quad (4)$$

where ε_o is the dielectric constant of free space (8.854×10^{12}). For PANI@ZnO-NPs/Zn^{2+}, σ is determined to be 1.1 ± 0.1 × 10^{-4} S m^{-1} to 3.0 ± 0.23 × 10^{-3} S m^{-1}. This value is quite high compared to the σ values obtained for PANI@AuNPs/Au^{3+} (8.6 ± 0.43 × 10^{-6} to 2.7 ± 0.21 × 10^{-5} S m^{-1}) and PANI0 (7.1 ± 0.31 × 10^{-6} S m^{-1} to 9.9 ± 0.27 × 10^{-5} S m^{-1}) under similar conditions.

Furthermore, the frequency dependent dielectric loss (dissipation factor) values tan δhave also been calculated in the same frequency range at room temperature (Fig. 11) and it was found that PANI@ZnO-NPs/Zn^{2+} always has a higher value compared to the solid PANI fibers (PANI@AuNPs/Au^{3+}) and nanoparticles (PANI0). The frequency dependence of the conductivity of PANI@ZnO-NPs/Zn^{2+} at different temperatures have also been measured, and this reveals the interesting result (Table 2) that conductivity decreases with higher temperature, due to the resistance caused by the lattice vibration and disturbance of the electronic resonance/hopping in the PANI backbone.

It is evident that the ac current conductivity σ is associated with the frequency-dependent ionic conductivity (σ_i) and electronic hopping (electronic resonance) conductivity (σ_e), *i.e.* $\sigma = \sigma_i + \sigma_e$. The frequency-dependent component σ_i is typical for the ionic conductivity of liquids.[41] The conductivity of PANI is predominantly associated with the frequency-dependant electronic hopping as it is known, and is not due to the occurrence of liquid in any structural form of PANI (see TGA plot, Fig. S3†). Therefore, it is worth mentioning that the high value of the frequency-dependent ac current conductivity (σ) of the PANI with rectangular hollow core [PANI@ZnO-NPs/Zn^{2+}] is a unique finding.

4 Conclusions

In conclusion, we prepared PANI nanotubes with rectangular hollow interior through a sonochemical method in the presence of a ZnO/Zn^{2+} system. This is the first report on polymer nanotubes with rectangular hollow interiors. The outer wall of the rectangular hollow tubes has been decorated with PANI nanobeads and triangular nanoflakes by a self-assembly

approach to obtain a "*Date-tree-like*" 3D structure. The frequency dependent conductance and the dielectric properties of the rectangular hollow PANI nanotubes have been investigated through impedance measurements, and excellent enhancement of these properties has been observed compared to the results obtained for solid PANI nanoparticles and solid nanofibers. Therefore, novel rectangular hollow PANI nanotubes with a rectangular hollow core, with surface decorated nanostructure, is a unique conducting polymer that can be used in various applications, such as for sensing, capacitance, electronic device fabrication *etc.* However, the mechanistic formation of the rectangular hollow core is assumed to occur through a self-assembly of PANI chains. Further detailed studies are needed in this direction to understand fully the reason for the formation of the rectangular hollow core of PANI. More detailed study towards this end will be reported elsewhere.

Acknowledgements

This work is supported by the University of Hyderabad (Central University) Start-up Grant (UH/F&A/2011-12/SG) and Department of Science and Technology (DST), India, Fast Track Grant for the Young Scientists (SR/FTP/ETA-00792011).

Notes and references

1 A. J. Heeger, *Angew. Chem., Int. Ed.*, 2001, **40**, 2591; A. G. MacDiarmid, *Angew. Chem., Int. Ed.*, 2001, **40**, 2581; H. Shirakawa, *Synth. Met.*, 2001, **125**, 3.

2 M. Angelopoulos, *IBM J. Res. Dev.*, 2001, **45**, 57; W. A. Gazotti, A. F. Nogueira, E. M. Girotto, L. Micaroni, M. Martini, S. D. Neves and M. De Paoli, *Handbook of Advanced Electronic and Photonic Material*, ed. H. S. Nalva, Academic Press, San Diego, CA, 2001, vol. 10, p. 53.

3 R. A. Bissell, K. C. Persaud and P. Travers, *Phys. Chem. Chem. Phys.*, 2002, **4**, 3482.

4 S. Geetha, C. R. K. Rao, M. Vijayan and D. C. Trivedi, *Anal. Chim. Acta*, 2006, **568**, 119.

5 P. M. George, D. A. LaVan, J. A. Burdick, C.-Y. Chen, E. Liang and R. Langer, *Adv. Mater.*, 2006, **18**, 577.

6 N. Oyama, T. Tatsuma, T. Sato and T. Sotomura, *Nature*, 1995, **373**, 598.

7 W.-C. Chen and T.-C. Wen, *J. Power Sources*, 2003, **117**, 273.

8 J. Huang and R. B. Kaner, *Angew. Chem., Int. Ed.*, 2004, **43**, 5817; R. B. Kaner, *ACS Nano*, 2008, **2**(9), 1841; H. D. Tran and R. B. Kaner, *Chem. Commun.*, 2006, 3915; X. Zhang and S. K. Manohar, *Chem. Commun.*, 2004, 2360.

9 R. Manda, V. Dasari, P. Sataranaya, N. V. Rasna, P. Paik and S. Dhara, *Appl. Phys. Lett.*, 2013, **103**, 141910.

10 P. Paik, Y. Mastai and A. Gedanken, *J. Mater. Chem.*, 2010, **20**, 4085; P. Paik, Y. Mastai and A. Gedanken, *Microporous Mesoporous Mater.*, 2010, **129**, 82; P. Paik, Y. Mastai and A. Gedanken, *ACS Appl. Mater. Interfaces*, 2009, **1**(8), 1834.

11 G. Wulff, *Angew. Chem., Int. Ed. Engl.*, 1995, **34**, 1812; T. Takeuchi and J. Haginaka, *J. Chromatogr., Biomed. Appl.*, 1999, **728**, 1; C. Alexander, H. S. Andersson, L. I. Andersson, R. J. Ansell, N. Kirsch, I. A. Nicholls, J. O'Mahony and M. J. Whitcombe, *J. Mol. Recognit.*, 2006, **19**, 106; A. Thomas and M. Antonietti, *Adv. Funct. Mater.*, 2003, **13**, 763; B. Wang, C. Chi, W. Shan, Y. H. Zhang, N. Ren, W. L. Yang and Y. Tang, *Angew. Chem., Int. Ed.*, 2006, **45**, 2088; S. Che, Z. Liu, T. Ohsuna, K. Sakamoto, O. Terasaki and T. Tatsumi, *Nature*, 2004, **429**, 281; S. Polarz and A. Kuschel, *Adv. Mater.*, 2006, **18**, 1206.

12 D. Chowdhury, *J. Phys. Chem. C*, 2011, **115**(28), 13554.

13 V. Svetlicic, A. J. Schmidt and L. L. Miller, *Chem. Mater.*, 1998, **10**, 3305; S. Sharma, C. Nirkhe, S. Pethkar and A. A. Athawale, *Sens. Actuators, B*, 2002, **85**, 131; I. G. Casella, T. R. I. Cataldi, A. Guerrieri and E. Desimoni, *Anal. Chim. Acta*, 1996, **335**, 217; G. Li, M. Josowicz, J. Janata and S. Semancik, *Appl. Phys. Lett.*, 2004, **85**, 1187; M. D. Shirsat, M. A. Banger, M. A. Deshusses, N. V. Myung and A. Mulchandani, *Appl. Phys. Lett.*, 2009, **94**, 083502; S. Virji, J. D. Fowler, C. Baker, J. Huang, R. B. Kaner and B. H. Weiller, *Small*, 2005, **1**, 624; J. Huang, S. Virji, B. H. Weiller and R. B. Kaner, *J. Am. Chem. Soc.*, 2003, **125**, 314; J. Wang, S. Chan, R. R. Calson, Y. Luo, G. Ge, R. S. Ries, J. R. Heath and H. R. Tseng, *Nano Lett.*, 2004, **4**, 1693.

14 C. G. Wu and T. Bein, *Science*, 1994, **264**, 1757; C. R. Martin, *Acc. Chem. Res.*, 1995, **28**, 61.

15 Z. X. Wei, Z. M. Zhang and M. X. Wan, *Langmuir*, 2002, **18**, 917; H. J. Qiu, M. X. Wan, B. Matthews and L. M. Dai, *Macromolecules*, 2001, **34**, 675; Z. M. Zhang, M. X. Wan and Y. Wei, *Adv. Funct. Mater.*, 2006, **16**, 1100; J. Jang and H. Yoon, *Langmuir*, 2005, **21**, 11484; M. G. Han and S. H. Foulger, *Small*, 2006, **2**, 1164; W. B. Zhong, S. M. Liu, X. H. Chen, Y. X. Wang and W. T. Yang, *Macromolecules*, 2006, **39**, 3224.

16 P. Anilkumar and M. Jayakannan, *Macromolecules*, 2007, **40**, 7311.

17 X. Y. Zhang, W. J. Goux and S. K. Manohar, *J. Am. Chem. Soc.*, 2004, **126**, 4502; X. Y. Zhang and S. K. Manohar, *J. Am. Chem. Soc.*, 2004, **126**, 12714.

18 Z. W. Niu, M. A. Bruckman, S. Q. Li, L. A. Lee, B. Lee, S. Pingali, P. Thiyagarajan and Q. Wang, *Langmuir*, 2007, **23**, 6719.

19 J. Stejskal and R. G. Gilbert, *Pure Appl. Chem.*, 2002, **74**, 857.

20 Z. Zhang, Z. Wei and M. Wan, *Macromolecules*, 2002, **35**, 5937; X. Lu, H. Mao, D. Chao, W. Zhang and Y. Wei, *Macromol. Chem. Phys.*, 2006, **207**, 2142; H. Qiu and M. Wan, *J. Polym. Sci., Part A: Polym. Chem.*, 2001, **39**, 3485; H. Qiu, M. Wan, B. Matthews and L. Dai, *Macromolecules*, 2001, **34**, 675; L. Zhang and M. Wan, *Nanotechnology*, 2002, **13**, 750; Z. Wei, Z. Zhang and M. Wan, *Langmuir*, 2002, **18**, 917; Y. Long, L. Zhang, Y. Ma, Z. Chen, N. Wang, Z. Zhang and M. Wan, *Macromol. Rapid Commun.*, 2003, **24**, 938; Y. Long, J. Luo, J. Xu, Z. Chen, L. Zhang, J. Li and M. Wan, *J. Phys.: Condens. Matter*, 2004, **16**, 1123; H. Xia, H. S. Chan, C. Xiao and D. Cheng, *Nanotechnology*, 2004, **15**, 1807; N. J. Pinto, P. L. Carrión, A. M. Ayala and M. Ortiz-Marciales, *Synth. Met.*, 2005, **148**, 271; Z. Zhang, Z. Wei, L. Zhang and M. Wan, *Acta Mater.*, 2005, **53**, 1373; L. Zhang and M. Wan, *Thin Solid Films*, 2005, **477**, 24;

H. Xia, J. Narayanan, D. Cheng, C. Xiao, X. Liu and H. S. O. Chan, *J. Phys. Chem. B*, 2005, **109**, 12677.

21 Y. S. Yang and M. X. Wan, *J. Mater. Chem.*, 2002, **12**, 897; L. Zhang and M. Wan, *Adv. Funct. Mater.*, 2003, **13**, 815; L. Zhang, Y. Long, Z. Chen and M. Wan, *Adv. Funct. Mater.*, 2004, **14**, 693; L. Zhang, H. Peng, Z. D. Zujovic, P. A. Kilmartin, C. Soeller and J. Travas-Sejdic, *Macromol. Chem. Phys.*, 2007, **208**, 1210; Q. Sun and Y. Deng, *Mater. Lett.*, 2008, **62**, 1831; Z. D. Zujovic, L. Zhang, G. A. Bowmaker, P. A. Kilmartin and J. Travas-Sejdic, *Macromolecules*, 2008, **41**, 3125; P. Petrov, P. Mokreva, C. Tsvetanov and L. Terlemezyan, *Colloid Polym. Sci.*, 2008, **286**, 691; Q. Sun, M. C. Park and J. Deng, *Mater. Chem. Phys.*, 2008, **110**, 276.

22 L. Zhang, H. Peng, C. F Hsu, P. A. Kilmartin and J. Travas-Sejdic, *Nanotechnology*, 2007, **18**, 115607; L. Zhang, H. Peng, P. A. Kilmartin, C. Soeller and J. Travas-Sejdic, *Electroanalysis*, 2007, **19**, 870; L. Zhang, H. Peng, J. Sui, P. A. Kilmartin and J. Travas-Sejdic, *Curr. Appl. Phys.*, 2008, **8**, 312.

23 Z. Wei, M. Wan, T. Lin and L. Dai, *Adv. Mater.*, 2003, **15**, 136.

24 C. Cheng, J. Jiang, R. Tang and F. Xi, *Synth. Met.*, 2004, **145**, 61.

25 L. Zhang and M. Wan, *J. Phys. Chem. B*, 2003, **107**, 6748.

26 J. Stejskal, P. Kratochvíl and A. D. Jenkins, *Polymer*, 1996, **37**, 367.

27 J. Kim, S. Kwon, S. H. Kim, C.-K. Lee, J. H. Lee, S. J. Cho, H.-S. Lee and H. Ihee, *J. Am. Chem. Soc.*, 2012, **134**, 20573.

28 D. Henry, D. Tran, Y. Wang, J. M. D'Arcy and R. B. Kaner, *ACS Nano*, 2008, **2**(9), 1841.

29 Q. Tang, J. Wu, X. Sun, Q. Li and J. Lin, *Langmuir*, 2009, **25**(9), 5253.

30 Y. S. Zhao, J. Xu, A. Peng, H. Fu, Y. Ma, L. Jiang and J. Yao, *Angew. Chem., Int. Ed.*, 2008, **47**, 7301; X. Zhang, X. Zhang, W. Shi, X. Meng, C. Lee and S. T. Lee, *Angew. Chem., Int. Ed.*, 2007, **46**, 1525; S. M. Yoon, I. C. Hwang, K. S. Kim and H. C. Choi, *Angew. Chem., Int. Ed.*, 2009, **48**, 2506.

31 J. Tang, X. Jing, B. Wang and F. Wang, *Synth. Met.*, 1988, **24**, 231; F. L. Lu, F. Wudl, M. Nowak and A. J. Heeger, *J. Am. Chem. Soc.*, 1986, **108**, 8311.

32 E. T. Kang, K. G. Neoh and K. L. Tan, *Prog. Polym. Sci.*, 1998, **23**, 277.

33 Z. M. Zhang, Z. X. Wei and M. X. Wan, *Macromolecules*, 2002, **35**, 5937.

34 W. Li, M. Zhu, Q. Zhang and D. Chen, *Appl. Phys. Lett.*, 2006, **89**, 103110.

35 J. P. Pouget, M. E. Jozefowicz, A. J. Epstein, X. Tang and A. G. MacDiarmid, *Macromolecules*, 1991, **24**, 779.

36 *Polymers and other Advanced Materials: Emerging Technologies and Business Opportunities*, ed. G. Louarn, S. Quillard, S. Lefrant and P. N. Prasad, Plenum, New York, 1995, p. 317.

37 J. X. Huang and R. B. Kaner, *Nat. Mater.*, 2004, **3**, 783.

38 G. Ćirić-Marjanović, V. Dondur, M. Milojević, M. Mojović, S. Mentus, A. Radulović, Z. Vuković and J. Stejskal, *Langmuir*, 2009, **25**(5), 3122; B. H. Kim, J. H. Jung, J. Joo, J. Kim and H. J. Choi, *J. Korean Phys. Soc.*, 2000, **36**, 366.

39 M. Iwamoto, *J. Appl. Phys.*, 1995, **77**, 5314.

40 J. R. Macdonald, *Impedance Spectroscopy*, Wiley-Interscience, New York, 1987, p. 66.

41 J. Frankel, *Kinetic theory of Liquids*, 1955, Dover, New York.

